Fifth International Symposium on Marine Propulsors
smp'17, Espoo, Finland, June 2017

Automated multi-objective optimization of ship propellers

John Huisman, Evert-Jan Foeth

Maritime Research Institute Netherlands (MARIN), Wageningen, The Netherlands.

ABSTRACT

A parametric propeller geometry model coupled to the genetic algorithm NSGA-II was used to optimize two propellers operating in a ship's wakefield. Both the radial distributions functions as well as radial sections were allowed to vary. For case 1 the propeller efficiency was maximized while the tip vortex noise as estimated by an empirical model was minimized. The pressure distribution was constrained by prescribing a margin against both suction and pressure side cavitation. A clear trade-off between both the tip vortex noise and efficiency was found. For case 2 the efficiency was maximized and the blade weight and thrust variations were minimized with a constraint on the maximum material stress following from load cases prescribed by the Finnish-Swedish ice-class rules. For this case (very) high skew propellers were found. The current optimization procedure can provide a well-balanced starting point for the design of high efficiency propellers while satisfying the conflicting requirements on cavitation inception, tip vortex nuisance, propeller-induced hull pressures fluctuations, weight and strength.

Keywords

Optimization, Propeller Design, Ice Class Rules

1 INTRODUCTION

MARIN focuses on a wide-range of propeller designs such as high-end "low-noise" propellers for yachts, delayed-cavitation inception designs for naval, research and cruise ships, low vibration-excitation or ducted propellers for special purpose vessels such as dredgers, tugs and fishing vessels. For most merchant ships, the best possible compromise between the propulsive efficiency and cavitation nuisance must be obtained, two objectives typically at odds.

Automated multi-objective optimization techniques are increasingly more suited for commercial propeller design projects (Brizzolara et al. (2009), Gaggero et al. (2015), Foeth (2015), Vesting (2016)). An optimization study, by exploring the design space, gives insight in the different trade-offs between conflicting objectives, indicates the influence of design constraints on the attainable objectives and shows the limits of attainable improvements.

In practice, the optimization procedure has not fully replaced manual design and the result can serve as an excellent starting point for the final propeller design.

This paper describes the methodology, strengths, weaknesses and practical applicability of a multi-objective optimization technique as applied to two cases. For case 1, optimization is applied to obtain maximum efficiency and to delay cavitation inception. In case 2 optimization of ice-class propellers is addressed, maximizing efficiency and minimizing blade weight, while satisfying the requirements from the Finish-Swedish ice-class rules.

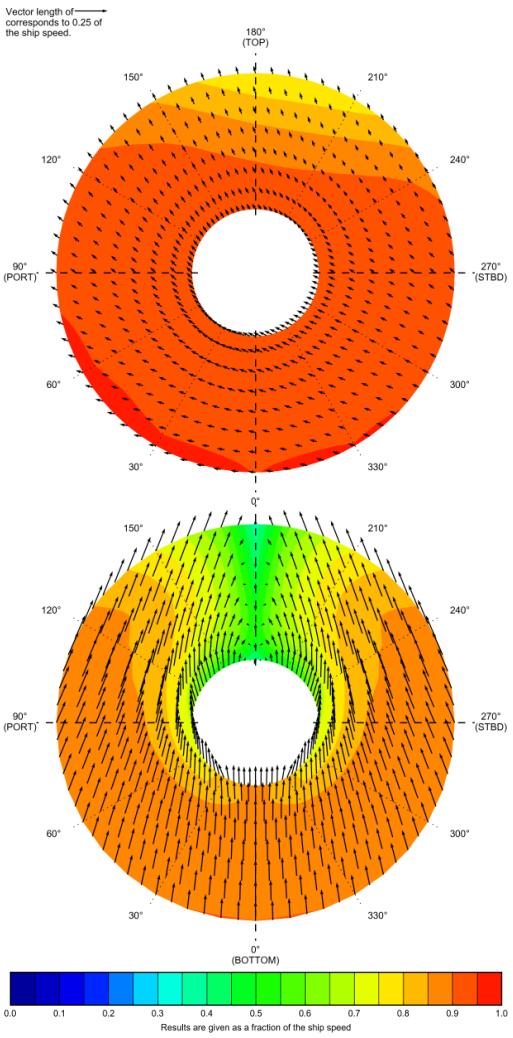

Figure 1: Wakefield for case 1 (top) and case 2 (bottom)

2 METHOD

MARIN's parametric propeller-geometry generator is coupled to a genetic algorithm and several analysis tools for both the hydrodynamic and structural performance, as described below. This computational framework has been named PropArt.

Genetic Algorithm

The genetic algorithm (GA) works along the principle of natural selection based on a series of optimization goals (evolutionary pressure) and population variation through cross-over and mutation of (genetic) information. Each individual is given a 'fitness value'; fitter individuals have a better chance of staying in the population and sharing their information with other fit members to procreate a new parameter set: offspring. Here the so-called Non-dominating Sorting Genetic Algorithm II (NSGA-II) by Deb et al. (2002) was used.

All results of a population are distributed in Pareto fronts that connect solutions that outperform each other on an equal number of goals and are equally fit. Pareto fronts are formed using individuals with an equal number of constraint violations, starting by designs without any violations. Some individuals violate geometrical constraints (e.g., CPP blades cannot pass each other) and are immediately replaced upon creation; most violations follow from analyzing the calculation results.

Each propeller can be analyzed by several analysis tools and for several conditions (e.g., both loaded and ballast draft). The first condition is termed the design condition and during this phase the mean pitch of the propeller is scaled to obtain the design thrust at a given rotation rate using a number of iterative (first steady and later unsteady) PROCAL computations [1]. The required thrust is thus not formulated as a constraint and the effective propeller pitch is a variable that was not set by the optimizer. For all other conditions the self-propulsion point can be determined by changing the rate of revolutions.

Analysis Tools

Propellers are analyzed for hydrodynamical performance using the Boundary Element Method (BEM) PROCAL (Bosschers et al, 2008) that computes the inviscid flow around the propeller. The calculations give the propeller performance in terms of thrust and power, the pressure distribution over the propeller blade surface and the extent and dynamics of the sheet cavitation.

The tip vortex noise is estimated with an Empirical Tip Vortex (ETV) model (Lafeber & Bosschers, (2015), Bosschers, 2017)), based on the circulation distribution as calculated by PROCAL. The pressures on the hull are analyzed by EXCALIBUR (van Wijngaarden, 2011) solving the 3D acoustic diffraction and scattering problems in the frequency domain using a surface panel method that uses PROCAL results as input to determine the pressure fluctuations of the first four of blade harmonics. All hydrodynamic tools have been developed and validated within the Cooperative Research Ships (CRS)[2].

The structural analysis of the propeller is performed by ANSYS, either using a quasi-steady approach for the propeller for the critical angular blade position in the propeller wake, or, by prescribing loads following ice-class rules.

Propeller Geometry

Both the radial and chordwise propeller distributions were parameterized by means of Bézier curves (e.g., Sederberg 2014) into optimization design variables (Foeth (2013, 2015), Park et al. 2015) for the radial distributions. The chordwise camber and thickness of the sections were either described by predefined sections modified by the radial thickness and camber functions or a Bézier (or spline) surface for the thickness and camber allowing for both a chordwise and a radial variation of blade sections (Mishima, 1996, Brizzolara et al. 2009). An example of a camber surface is given in Figure 2: both the radial camber distribution and the chordwise distribution were specified. Typically, a complete propeller parameterization resulted in 40 to 45 design variables.

PROCAL is an inviscid method and boundary-layer separation cannot be calculated directly. The trailing edge geometry is constrained by penalizing high adverse pressure gradients in the pressure recovery region to avoid separation; no actual separation criterion was implemented (yet). An empirical value $dp/dc \leq 27$ was applied as constraint.

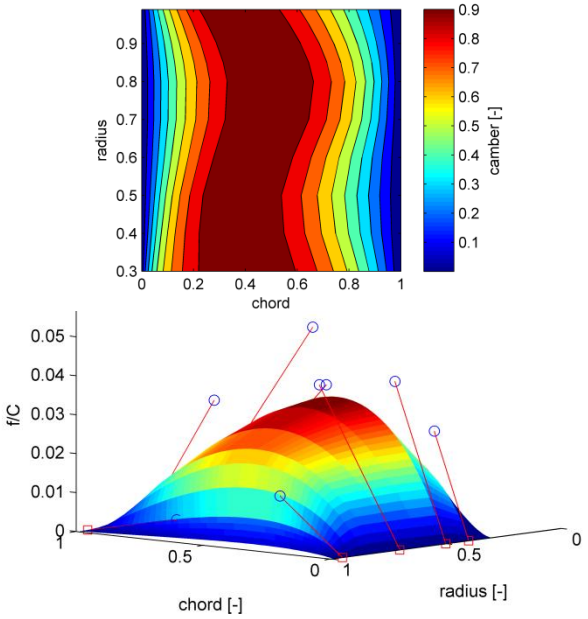

Figure 2: Example of the propeller camber parameterized by a Bézier surface with normalized camber (top) and 3D view of f/C (bottom).

[1] The rotation rate can be an optimization parameter, but was fixed in the present work.

[2] http://www.crships.org/

3 NON-CAVITATING PROPELLER OPTIMIZATION

Yachts and cruise vessels typically require non-cavitating propellers up to 100% Maximum Continuous power Rating (MCR) for optimal comfort. Optimization of such propellers is focused on reducing inboard noise and vibrations by prescribing a small margin against sheet cavitation while delaying the inception of tip vortex cavitation. Unsteady fully-wetted PROCAL computations within the ships wakefield were performed. A nominal, computed full-scale wakefield was used as given in Figure 1. The results of the optimization were compared with a reference propeller.

The pressure coefficient, CPN, based on the rotation speed, is defined as

$$CPN = \frac{p_s - p}{\frac{1}{2}\rho n^2 D^2} \tag{1}$$

with p the local pressure on the blade surface, p_s the total pressure at the shaft depth, and ρ, n and D, the fluid density, the propeller rate of revolutions and diameter, respectively. As such, CPN can directly be compared with the cavitation number σ_N at 100% MCR. The margin of the pressure reserve in the flow versus the dynamic pressure as a function of rotation speed is expressed as the cavitation number

$$\sigma_N = \frac{p_s - p_v}{\frac{1}{2}\rho n^2 D^2} \tag{2}$$

with p_v the vapor pressure. Inception of cavitation is assumed to occur when $\sigma_N = -C_{PN}$. The margin against cavitation as used in the optimization is defined as:

$$\Delta\sigma_N \equiv \frac{\min(-C_{PN}) + \sigma_N}{\sigma_N} \tag{3}$$

The objectives of the optimization were to maximize efficiency and reserve margin against sheet and bubble cavitation inception using eq.(3). This margin against cavitation inception was obtained from the unsteady, fully-wetted pressure distributions on the propeller blade throughout rotation in the ship's wake.

The (source) noise level of the cavitating tip vortex formed a second constraint at a maximum level of 168.5 dB re 1 uPa^{2}m^2, that is, 3dB lower than calculated for the reference propeller.

This optimization was performed with 64 generations of 160 propellers for a single condition; 100% MCR. Computations are performed on a computational cluster computing all propellers simultaneously.

Cavitation Margin

The trade-off between efficiency and the margin against cavitation is visualized in Figure 3 as a function of the generation number.

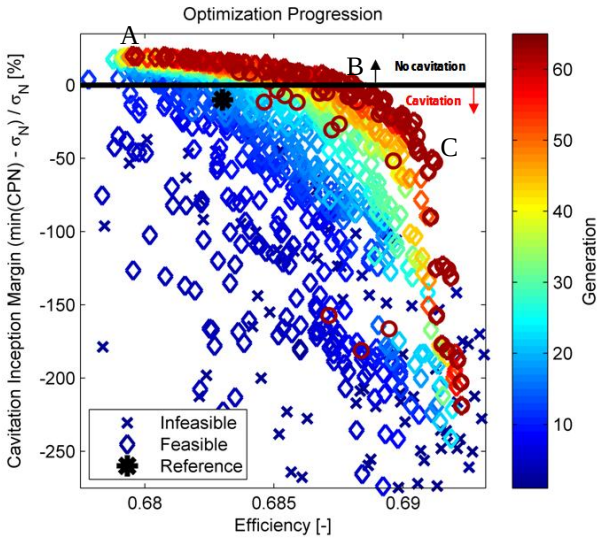

Figure 3: Optimization results for case 1 showing the margin against cavitation inception and efficiency.

All other colored markers represent the performance of a propeller within the optimization. The successive Pareto fronts as presented by the color scale show the progression of the optimization. Some propellers did not satisfy one or more constraints and are marked by 'x' as infeasible; these solutions were unlikely to be used in the determination of the next generation. The optimization converged towards the final Pareto front as shown in red; some propellers were free of cavitation at the cost of lower efficiency, and some had higher efficiency at the cost of cavitation. A manual selection of the 'optimum' propeller is still required.

Within the Pareto front, three propellers were elected for further analysis that could serve as starting point for the final propeller design. Figure 4 presents the highest efficiency propellers featuring about 20% (propA), 5% (propB) and -30% (propC) cavitation margin as defined in eq. (3).

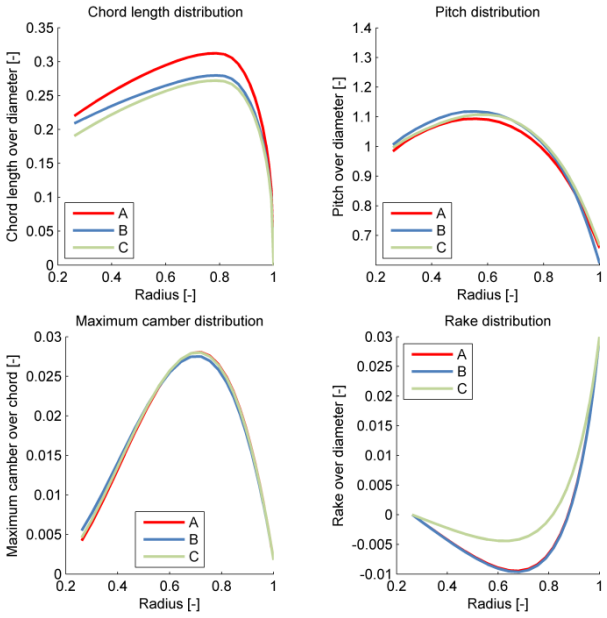

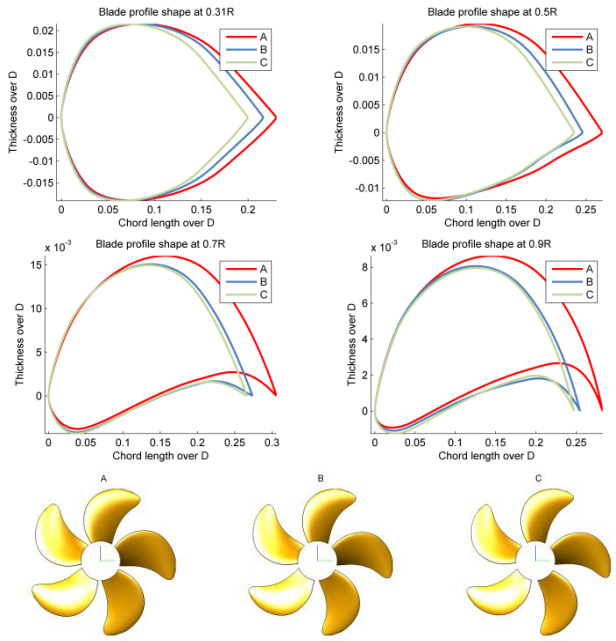

Figure 4: Geometry comparison for the selected propellers along the Pareto front. Maximum thickness and skew have not been taken into account in the optimization and are taken constant.

Comparing the propeller geometries as presented in Figure 4 the following is observed:

- The cavitation objective steers towards the same camber-over-chord ratio distribution.
- The low-aspect ratio sections at the hub are not very sensitive to the cavitation objective and these sections did not evolve towards well-rounded leading edges.
- At higher radii the cavitation criterion put evolutionary pressure on obtaining smooth leading edges.

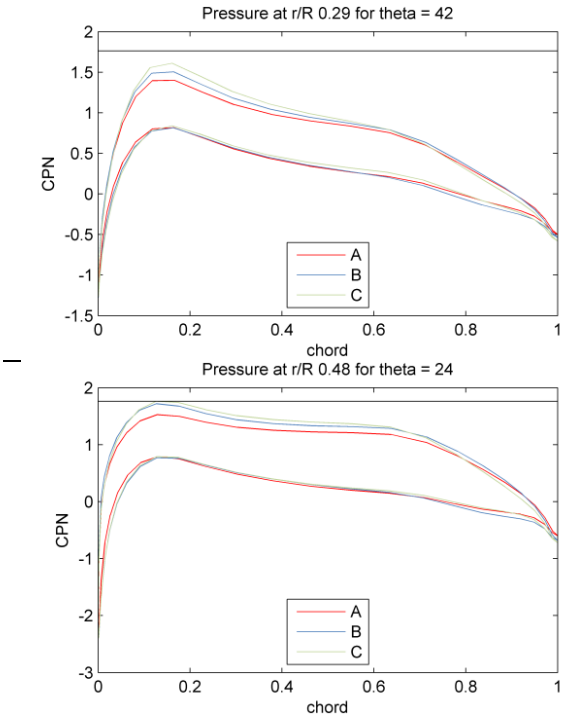

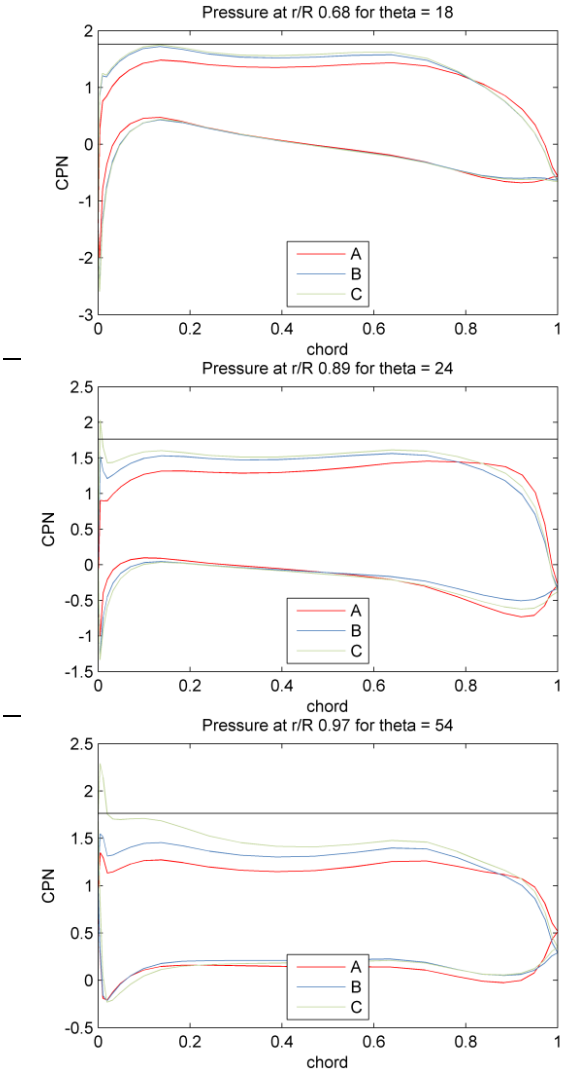

Figure 5: Comparison of pressure distributions for the selected propellers along the Pareto front.

Referring to Figure 4 and Figure 5 the following is remarked:

- The section profiles at higher radii were optimized to have a near-constant pressure distribution. As shown, this is not yet optimally reached with the 64 generations as used in this optimization case or not yet possible with the current implementation of the sectional thickness. Especially in the tip region, the pressure could have been smoothed out further, but at the cost of higher computational costs and longer running times.
- The pressure recovery at r/R = 0.89 for propA seems not to be physical. A better separation avoidance criterion is still required to really exploit the objectives with free section shapes.

Performing such an optimization gives insight in the trade-off between cavitation and efficiency. In addition, custom blade sectional profiles were obtained that are balanced for efficiency and cavitation inception delay. Furthermore, the radial loading distribution is optimized for maximum efficiency.

Tip Vortex Noise

In a second optimization study of the same case the cavitation margin was set at 5% as constraint. The ETV level was implemented as a minimization objective. The trade-off between maximum efficiency and lowest tip vortex noise is given in Figure 6. The reference propeller is plotted again with the black star. Two propellers, A and B, are elected for further analysis, see Figure 7.

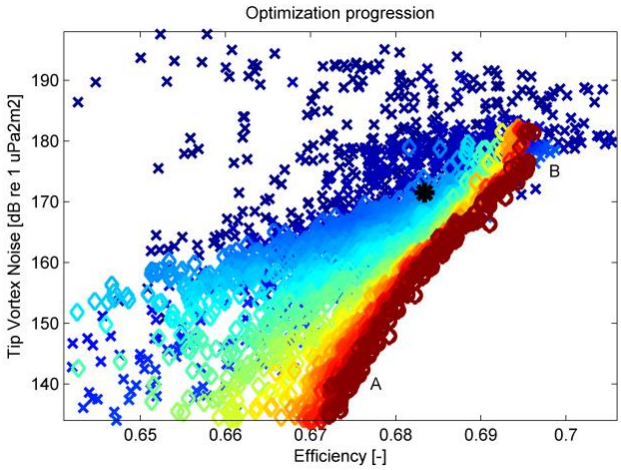

Figure 6: Trade-off between efficiency and ETV tip source noise level

A clear relation between efficiency and tip vortex noise is observed. Two propellers from the front were selected with the pitch, camber, chord and circulation distribution presented in Figure 7. The tip vortex strength depends on the circulation gradient at the tip. As expected the lower-noise propeller design (A) shows more tip unloading by means of a lower pitch at the tip and lower camber-to-chord ratio, detrimental to the efficiency: the circulation (gradient) in the tip region of the propeller is reduced, which reduces the strength and noise levels of the tip vortex. While propeller (B) was constrained by the cavitation inception margin, propeller (A) is driven by the tip vortex noise objective featuring almost 15% margin against cavitation inception.

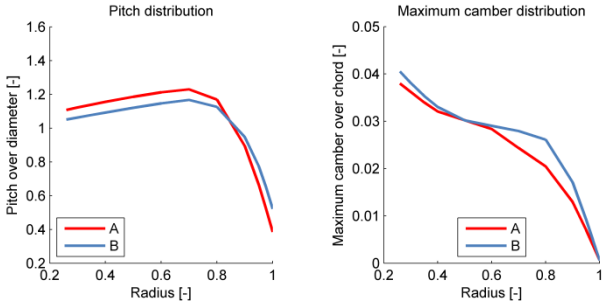

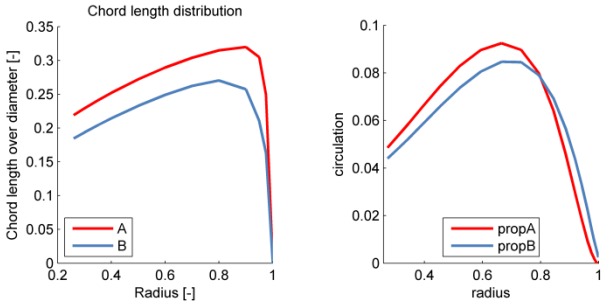

Figure 7: Comparison of pitch, camber and chord length for a low (A) and higher tip vortex noise propeller (B).

Hull Pressures

In a third optimization of the same case the minimization of the non-cavitating hull pressures was applied. Figure 8 shows that no propellers could be obtained that satisfy the 5% cavitation margin: the optimization quickly converged towards propellers with reduced chord length in the tip (i.e. lower position of the maximum chord) which feature smaller hull-pressure pulses but cannot satisfy the cavitation constraint. In this case the skew angle was fixed, leaving it as a free variable may have resulted in convergence of the optimization problem, but maybe at the cost of stronger leading edge vortices due to increased skew.

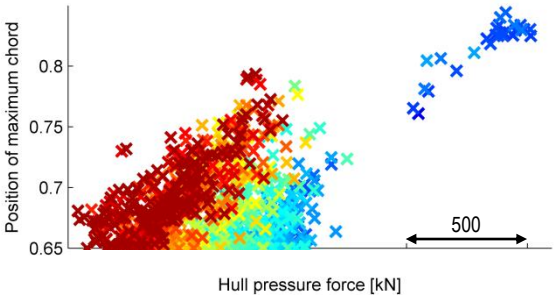

Figure 8: Optimization result showing the dependency between the position of maximum chord and the hull pressure force.

4 ICE CLASS PROPELLER OPTIMIZATION

For the second optimization case a propeller for the chemical tanker from the EU project Streamline (van der Ploeg et al. 2013) was optimized taking the Finish-Swedish Ice-Class Rules in account. For this case the propeller efficiency was maximized while the blade mass and thrust variation were minimized. The thrust variation is defined in this case as the amplitude of the variation of the thrust coefficient during the blade rotation. Minimization of the thrust variation typically leads to high skew values while the strength requirements typically lead to very low skew values.

Structural Strength

Usually the structural integrity is taken into account in an optimization by prescribing the thickness and limiting rake and skew following the regulations of the classification society. For ice-class propellers structural analyses are required and the strength requirements lead

to an increase in blade weight and can influence the hydrodynamic performance considerably.

Ice-class rules specify the maximum lifetime ice-loads (Trafi, 2010) applied on the propeller blade by means of the five Load Cases (LC1 to LC5). For each load case a different design load should be analyzed by a Finite Element Method (FEM) stress analysis. The design forces Fb and Ff as defined in the ice-class rules were distributed as a uniform pressure applied on a certain area of the propeller blade for both backward (force Fb) and forward bending (force Ff), see Figure 9. For a fixed pitch propeller, the trailing edge should be loaded on the pressure side to account for backing operations in ice.

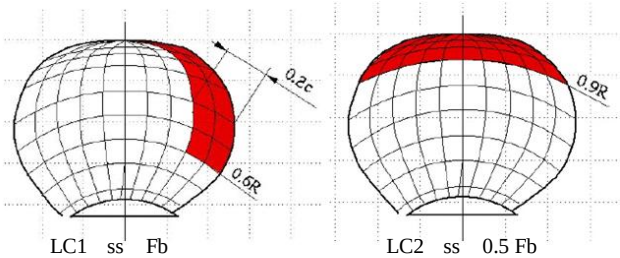

Figure 9: Load cases (LC) as defined by the ice-class rules with backward-bending load Fb, forward-bending load Ff applied on either the suction (ss) or pressure side (ps). LC5 is applied on the trailing edge.

Three physical phenomena are considered within the ice-class design loads, as explained by Browne & Norhamo (2006):

1. Ice-milling, the ice-contact process where the blades sequentially cut through the ice with leading or trailing edge. A regression analysis on the calculated unsteady loads for a non-skewed ice-class propeller using Soininen's model for ice-milling loads (Soininen, 1998) yields the backward bending force (Koskinen et al., 1996). This suction load is prescribed in the first load case of the ice-class rules.
2. Ice-blockage: the hydrodynamic effect by the proximity of blocks of ice near the leading edge. This hydrodynamic disturbance load is based on full-scale measurements and prescribed for the third load case. Although the load acts on the suction side, the load is applied to the pressure side in load case three.
3. Propeller-tip buckling. To account for buckling of the tip of high-skew ice-class propellers Norhamo et al., (2009) showed by reverse engineering with FEM analyses that tip load cases should be considered: 50% of the backward and forward bending load are applied for the second and fourth load case respectively.

Within the optimization procedure, a FEM analysis using structured, linear shell elements is applied. A mesh refinement study following the procedure of Eça & Hoekstra (2014), showed that a structured mesh of 40x50 shell elements in radial and chordwise direction gives similar results within 1.4% accuracy compared to a dense unstructured solid model. For optimization purposes, a surface description is preferred: the same paneling routine as used for the grid generation of PROCAL is used to generate the mid-chord surface with prescribed thickness.

The maximum material stress resulting from any of the five load cases should not exceed allowable stress. This was applied as optimization constraint.

Results

PropArt searches for propellers that satisfy the stress constraints from the five load cases of the ice-class rules, while optimizing for minimum mass, minimum thrust variation and maximum efficiency. Figure 10 shows the progression of the optimization. Each marker represents the performance of a propeller geometry in terms of the objectives and the colors indicate the generation number showing the formation of a Pareto front. All propellers that do not meet one of the ice-class load-case constraints are marked by a cross.

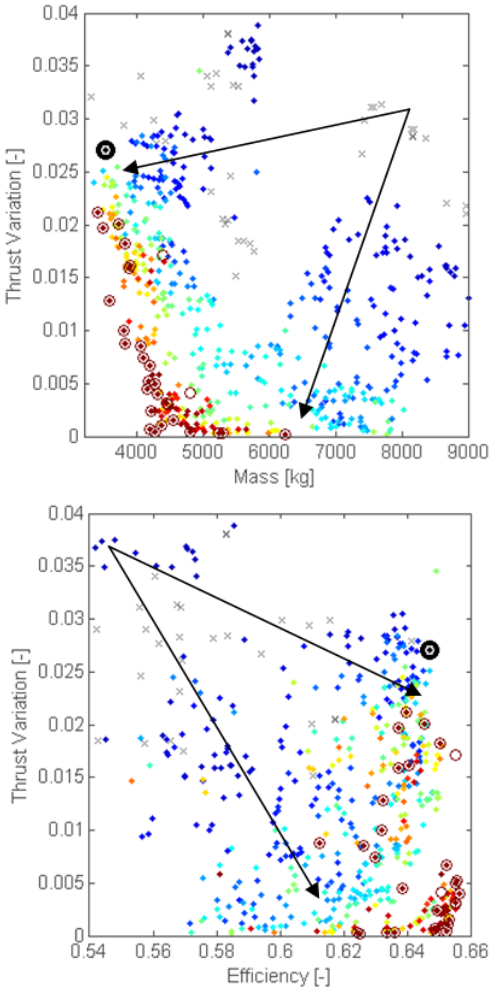

Figure 10: Optimization results for ice-class propellers.

No propellers are shown that violate the ice class constraint for the later generations, however, many unfeasible propellers were generated with each new generation, but as each successive Pareto front was formed by propellers with the best fitness, the unfeasible designs were typically discarded immediately. The

current implementation of PropArt does not take the degree of the constraint violation into account and thus the Pareto front is approached from the feasible design space only.

Figure 11 shows the parameterized geometry of one of the propellers in the group from the bottom corner of Figure 10. The material-stress contours for the five load cases from the ice-class rules are given in Figure 12. None of the ice-class load cases is critical with respect to the maximum allowable material stress of 299 MPa. The maximum stress occurs for load case four (LC4) in the mid-chord tip region of the blade as 260 MPa.

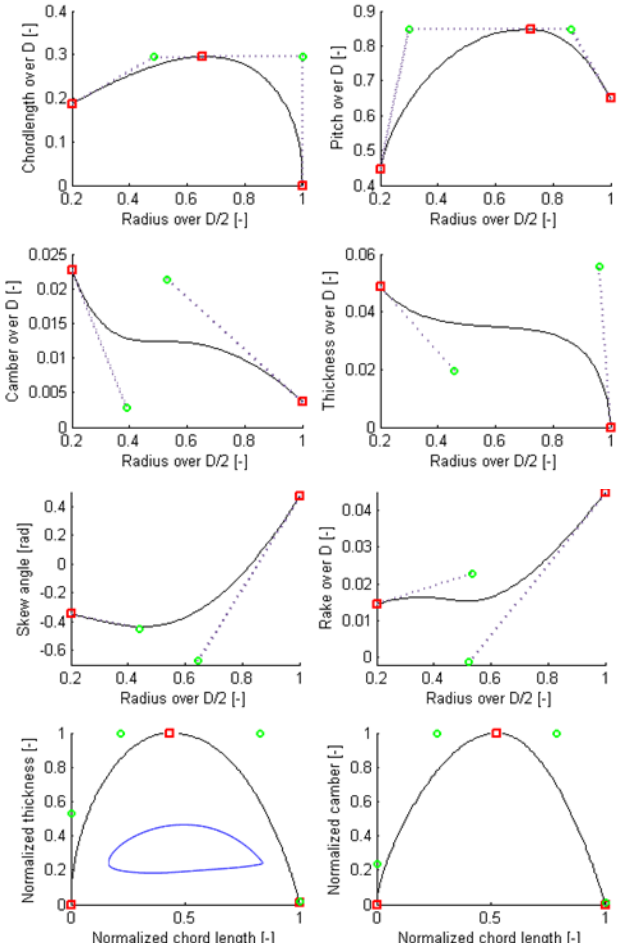

Figure 11: Overview of propeller distributions for one of the best propellers. The green circles and red squares represent the control points of the Bézier curves. A sketch of the resulting blade profile at 0.7R is given inside the chordwise thickness distribution.

For all propellers on the Pareto Front a high skew angle up to 50 degrees was found. It was expected that the optimization problem would show a trade-off between the required ice-class strength and blade weight as a function of the skew angle, however, propellers with the same mass and efficiency as the target propeller (without ice-class) are found with a much lower trust variation due to the skew angle. This shows that PropArt finds very highly skewed propellers which do satisfy the ice-class stress constraints. Note that thickness remains large towards the propeller tip. Due to increased skew, more thickness is required in the tip region to satisfy the stress constraint.

High-skew fixed-pitch propellers are prone to ice damages during backing with the trailing edge of the tip hitting the ice first (Norhamo et al., 2009). The load distribution as described by the ice-class rules with most of the load distributed along the trailing edge does not seem applicable for high skew. A slight redistribution of the ice loading of these propellers quickly leads to stresses exceeding the maximum. The presented optimized propellers presented are not robust designs and will never be produced in practice. If the skew angle is limited based on experience with ice-class propellers, the optimization is however suitable to provide a starting point for a low-weight ice-class propeller design.

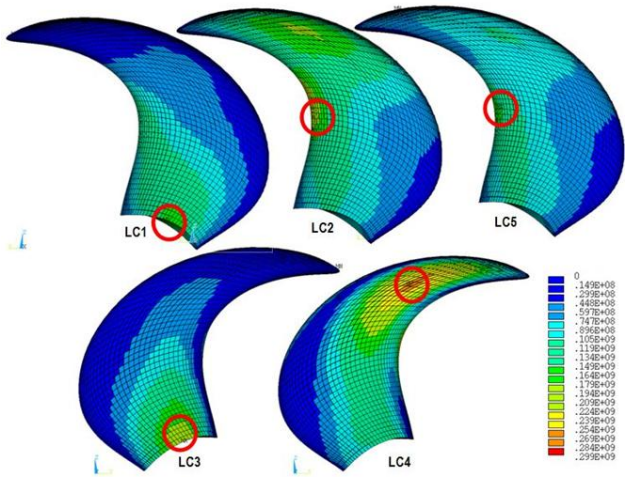

Figure 12: Von Mises stress contours in [MPa]. None of the ice-class load cases is critical. The red circles indicate the position of maximum stress.

5 CONCLUSIONS

A parametric propeller geometry model coupled to the genetic algorithm NSGA-II was used to optimize two propellers operating in a ship's wakefield. Both the radial distributions functions for pitch, skew, rake and chord, as well as radially varying chordwise camber and thickness of the sections were allowed to vary. A FEM implementation based on linear shell elements was coupled to PropArt applying the load prescribed by the ice-class rules.

For case 1 the propeller efficiency was maximized while the tip vortex noise as estimated by an empirical model was minimized. The pressure distribution was constrained by prescribing a margin against both suction and pressure side cavitation. A clear trade-off between the tip vortex noise and efficiency was quantified.

For case 2 the efficiency was maximized and the blade weight and thrust variations minimized with a constraint on the maximum material stress following from load cases prescribed by the Finnish-Swedish ice-class rules. For this case (very) high skew propellers were found.

While these propellers meet the ice-class rules for the same weight and efficiency as the non-ice-class reference propeller, they are not very robust against small changes in the distribution of the ice force on the blades. The optimization procedure may require a limit on the skew angle currently not specified in the ice class rules.

Optimization procedures may blindly exploit the limitations the analysis tools or limitations as set by the goals and constraints. Clearly, the advantage of quickly exploring a much larger parameter space than would be possible during the manual design process is offset by shifting the designer's attention towards the engineering of a robust environment for the optimization.

The current optimization procedure can provide a well-balanced starting point for the design of high efficiency propellers while satisfying the conflicting requirements on cavitation inception, tip vortex nuisance, propeller-induced hull pressures fluctuations, weight and strength. Our future efforts will be directed at improved parameterization of the hydrodynamical sections and criteria for sheet cavitation noise and erosion.

For the future outlook in the development of PropArt, the following is remarked:

- By using a cavitation and pressure gradient constraint, the chordwise thickness and camber distributions using two generic Bézier curves evolved towards a natural sectional description. However, these generic curves cannot describe all sections typically applied to propeller design and the use of parametric chordwise camber and thickness distributions may offer further improvements.
- The heuristic pressure gradient restriction in the pressure recovery region over-constrains the section design. Using either an inviscid 3D boundary-layer separation model or integrating a RANS calculation into the optimization loop would result in a more physics-based criterion.

REFERENCES

Bosschers J., Vaz, G., Starke A.R., & Wijngaarden E. van, (2008). 'Computational analysis of propeller sheet cavitation and propeller-ship interaction', RINA CFD Marine CFD, 2008, Southampton, UK.

Bosschers, J. (2017). A Semi-Empirical Method to Predict Broadband Pressure Fluctuations and Underwater Radiated Noise of Cavitating Tip Vortices. Proceedings of the Fifth International Symposium on Marine Propulsors, Espoo, Finland.

Brizzolara, S., Gaggero, S. (2009). 'Silent propellers with unconventional profile shapes. Examples obtained with a new automatic optimization method.' Proceedings of the 4th Annual Conference MAST2009 on Maritime Systems and Technology. Stockholm, Sweden.

Browne, R.P. & Norhamo, L. (2006). 'IACS Unified Requirements for Polar Ships – Background notes to "Propeller Ice Interaction Loads"'. IACS UR I3 **15**, Rev 0.1.

Deb, K., Pratap, A., Agarwal, S. & Mayarivan, T. (2002). A fast and Elitist Multiobjective Genetic Algorithm: NSGA-II. IEEE Transactions on Evolutionary Computation **6**(2), pp. 182 – 197.

Eça, L. & Hoekstra, M. (2014). A procedure for the estimation of the numerical uncertainty of CFD calculations based on grid refinement studies. Journal of Computational Physics **262**, pp. 104-130.

Foeth, E.J. (2015). Systematic propeller optimization using an unsteady Boundary Element Method. Proceedings of the Fourth International Symposium on Marine Propulsors, Austin, Texas, USA.

Gaggero, S., Viviani, M., Adalid, J.G., Sobirno, M.P., Gennaro, G., Sanguinetti, & M., Bina, G. (2015). A design by optimization of tip loaded propellers, Proceedings of the Fourth International Symposium on Marine Propulsors. Austin, Texas, USA.

Koskinen, P., Jussila, M. & Soininen, H. (1996). 'Propeller ice load models'. Technical Research Centre of Finland (VTT). Research Notes, no. 1739.

Lafeber, F.H., Bosschers, J. (2015), 'Computational and Experimental Prediction of Propeller Cavitation Noise'. Proceedings of OCEANS'15, Genova, Italy.

Mishima, S. (1996), 'Design of cavitation propeller blades in non-unifrom flow by numerical optimization', PhD thesis. Massachusetts Institute of Technology.

Norhamo, L., Bakken, G. M., Deinboll, O. & Iseskär, J.J. (2009). 'Challenges related to propulsor – ice interaction in arctic waters'. Proceedings of the First International Symposium on Marine Propulsors. Trondheim, Norway.

Park, J.Y., Peric, M., & Park, D., 'An optimization process for propeller design and its application based on CFD', 25th International Ocean and Polar Engineering Conference, Kona, Hawaii, USA, June 2015.

Ploeg, A. van der & Foeth, E.J. (2013). Optimization of a chemical tanker and propeller with CFD. Proceedings of the 5th International Conference on Computational Methods in Marine Engineering. Hamburg, Germany.

Soininen, H. (1998). 'A propeller-ice contact model'. PhD thesis. Espoo: VTT publications, Finland.

Trafi (2010). 'Maritime safety regulation - Ice class regulations and the application thereof', issued 23 November 2010 by the Finnish Transport Safety Agency. TRAFI/31298/03.04.01.00/2010.

Vesting. F., Gustavsson, R., & Bensow, R.E., Development and application of optimization algorithms for propeller design, Ship Technology Research **63**.

Wijngaarden, H.C.J. van. (2011). Prediction of Propeller-Induced Hull-Pressure Fluctuations. PhD dissertation. Wageningen: MARIN, The Netherlands.